# Monte Carlo investigation of secondary particles production in soft tissue during carbon ion therapy by GEANT4 toolkit and MCNPX Code

Ali Nouraddini-Shahabadi[a], Mohammad Reza Rezaie[b,*], Saeed Mohammadi[a]

[a] *Department of Physics, Payame Noor University, P. O. Box 19395-3697, Tehran, Iran*
[b] *Department of Nuclear Engineering, Faculty of Sciences and Modern Technologies, Graduate University of Advanced Technology, Kerman, Iran*

H I G H L I G H T S

- Secondary particle production of carbon ions in soft tissue by Geant4 toolkit and MCNPX code.
- Calculation of radioactive elements production by carbon ions in soft tissue.
- Calculation the range, beam divergence and beam Tail of carbon ion in soft tissue.
- Calculation of secondary particle Dosimetry production by carbon ion in soft tissue.

A B S T R A C T

High-energy heavy ions produced by accelerators are used in industrial and medical applications. Recently carbon ions have been used in the treatment of cancerous tumors. Heavy ions by the spallation process will activate the soft tissue components before tumors. In this research by GEANT4 toolkit and MCNPX code simulation were tried to calculate the secondary particles and radioactive elements produced in the soft tissue around tumors by the carbon ions spallation process. In the MCNPX code, the F8 tally card with the FT8 command was used to extract the activation and spallation information of secondary particles in the $Z_1=1$ to $Z_2=25$ atomic numbers range. It was shown that a wide range of radioactive elements was produced in healthy tissues in carbon therapy. In addition to produced secondary particles, the Be-10 and C-14 radioactive elements were produced in high-energy carbon ions in soft tissue. Also, the GEANT4 toolkit result of produced secondary particles dosimetry was shown that the secondary particles dose per carbon ion is between 1.66 to 33.54 nGy for carbon ion energy between 1140 to 5160 MeV. The tail for 3480, 4080, and 5160 MeV of carbon ion energy are 0.12, 1.01, and 11 cm respectively. The carbon ion beam divergence increases with beam energy and achieve to 33 mm for 5160 MeV carbon ion.

## 1 Introduction

Various methods are used for the treatment of cancerous tumors, such as surgery, laser radiation, brachytherapy, nuclear radiation , heavy ion radiation therapy, chemotherapy, etc. (Sudhakar, 2009; Kramer-Marek and Capala, 2012; Wang et al., 2021; Gogineni et al., 2021; Kayani et al., 2021; Lin et al., 2010; Allodji et al., 2021). Heavy ion accelerators have many applications in radiation therapy (Jablonska et al., 2021; Loap and Kirova, 2021; Ho et al., 2020; Chen and Paul, 2007; Schippers et al., 2006; Pasler et al., 2011; Liu et al., 2011; Iwata et al., 2023; Song et al., 2023). Recently, the possibility of using high-energy ions that are accelerated by certain techniques in the treatment of cancerous tumors has been investigated in various laboratories (Kasesaz et al., 2014; Anikin et al., 2020; Sauerwein et al., 2011; Hassanein et al., 2018; Cheng and Feng, 2021; Didi et al., 2019). When heavy charged particles pass through human tissues, the linear energy transfer (LET) is very high due to its high stopping power (de Freitas Nascimento et al., 2022). Although most of the ion energy is left in the Bragg peak, the energy transfer along the path to the Bragg peak location is also high due to the high energy of the particles (Oancea et al., 2023).

The carbon ion beam is a good candidate for tumor

therapy because of its excellent depth-dose characteristics combined with increased biological efficiency (RBE) and reduced oxygen effect in the Bragg peak region (Masunaga et al., 2010; Jäkel, 2020). Some limitation in the application of carbon ion beams is that the spallation process along the beam path in tissue that leads to an attenuation of the carbon ion flux and produces secondary particles (Pshenichnov et al., 2005). The dose distribution of the carbon ion beam is changed through the presence of secondary particles. Without secondary particles, the biological effect in the target volume is reduced because only a fraction of the carbon ion reach the Bragg peak region (Ounoughi et al., 2022). Therefore, the information about secondary particles is essential for the determination of the additional dose in carbon ion tumor treatment. So far, there are only a few experimental data on secondary particles for light ions in water (Kramer-Marek and Capala, 2012)7. With information about secondary particle production by carbon ion beam, it can be investigated the radioactive elements produced in soft tissue, the tail of the carbon beam in Bragg peak, and the additional dose along the stopping path. In addition to the possibility of increasing temperature and molecular degradation in the composition of body tissues, it is possible to perform nuclear interactions with the tissue elements. In this interaction, the nucleus becomes a compound nucleus by absorbing a charged particle before it decays in different modes such as the emission of photons, neutrons, alpha, and heavier particles (Chhura et al., 2022). The produced photons or gamma rays also affect other tissues and by producing neutrons due to the photoneutron process, they cause more radiation hazards to the patient body. One of the most important processes of heavy ion interaction with the nuclei of the elements that can damage the tissue materials is the possibility of the spallation process. In the spallation process, the nucleus evaporates by the capture of incident ion and it change to a set of radioactive and nonradioactive elements with a mass number less than the target (Luo et al., 2023). The spallation process occurs when the energy of the incident ion is higher than a certain threshold for each element. In ion therapy, the energy of the particles is generally greater than the energy of the spallation threshold, which depends on the binding energy of the target nucleus, and therefore spallation interaction occurs. In the spallation process with high energy charged particles, due to the energy transfer to the target nucleus, evaporation takes place, and a wide range of elements with a mass number less than the target nucleus is produced (Yoo, 1998). Recently it is possible to produce different heavy ions such as carbon up to 3.5 TeV energy (Williams et al., 2023; Zakalek et al., 2020; Stankovsky et al., 2001; Washio et al., 2011; Jowett, 2016). In the direct application of heavy ions, high-energy ions have already been used to treat tumors in various organs. High energy ions, due to their Bragg peaks, transfer more energy to the tumor than to healthy organs (Alanazi et al., 2022). In this work, using the GEANT4 toolkit, it was tried to investigate the possibility of producing secondary particles as a result of the interaction of carbon ions with soft tissue, the radioactive elements produced in soft tissue, the tail of carbon

beam in Bragg peak, the divergence of carbon ion beam and the additional dose along the stopping path. Monte Carlo simulation is a precise method to confirm the results and develop and optimize a test sample. GEANT4 toolkit (taken from Geometry and Tracking), is a Monte Carlo simulation toolkit written in C++ programming language and based on the transport of various types of particles in the environment. In this research, by ions irradiation on soft tissue, the degree of activation of soft tissue is examined and the benefit of producing radioisotopes produced in it is determined using the MCNPX code and GEANT4 toolkit. The MCNPX code is a nuclear code based on the Monte Carlo method (Khezripour et al., 2017). Also, due to the direct use of carbon ions in the treatment of internal tumors of the body, the amount of spallation of these heavy ions and radioactive elements produced in the soft tissue of the body is investigated.

## 2 Materials and methods

### 2.1 MCNPX simulation of secondary particle production by carbon ions interaction with soft tissue

In this study version 2.7.E of the MCNPX code was used to build a Monte Carlo model for heavy-ion therapy. The input file of MCNPX codes include the geometry cards, surface cards, and data cards. The geometry of the cells consists of the soft tissue ia s sphere with 2 cm radius. In the data card section, the information on the percentage of elements, the information on heavy ion's source energy, as well as how to extract spallation data are given. The F8 tally card with the FT8 command was used to extract the activation and spallation information. The FT8 command is expressed as FT8 Res Z1 Z2. RES shows the yield of spallation and activation in the Z1 to Z2 atomic numbers interval. Also, beam current can be obtained using F1 tally. The output file of the MCNP code contains a lot of information that the user can use to extract the required data. The results of typical MCNPX code include the number of simulated particles, the mean, error, variance of variance (VOV), and Figure Of Merit (FOM) to assist the user for checking the statistical behavior of the obtained result.

In this study, for extracting the interaction, activation, and spallation products, the output of the F8 tally is different from the normal case. The output of the FT8 tally includes the atomic and mass number of the generated element and the element generation yield due to the spallation process. The yield of the spallation process is an equal ratio of the mass of the element produced per one source particle to the mass of the irradiated element. By extracting the produced elements data by the spallation process, the yield of the radioactive elements can be obtained with using the table of radioisotopes. In the results section, the data related to the produced radioactive elements are mentioned. The high energy sources of 12C ion were examined in the soft tissue, which is healthy tissue before the treatment of internal tumors, and the number of radioactive elements produced in them was calculated.

**Table 1:** Comparison of practical carbon ion range in water with GEANT4 toolkit and MCNPX result.

| Carbon Energy MeV.u$^{-1}$ | 195 2340 (MeV) | 270 3240 (MeV) | 281 3372 (MeV) | 392 4704 (MeV) |
|---|---|---|---|---|
| Range (cm) (Suit et al., 2010) | 8 | 14.15 | 15 | 27 |
| Range (cm), MCNPX results | 8.25±0.08 | 14.50±0.15 | 15.50±0.16 | 26.75±0.27 |
| Range (cm), GEANT4 toolkit results | 8.10±0.08 | 14.20±0.14 | 15.10 ± 0.15 | 26.70±0.27 |

The geometry of the problem, in this case, is a soft tissue cylinder with a radius of 2 cm and variable thickness as Fig. 1. The energy of the carbon ion source is between 1140 to 5160 MeV that listed in Table 1.
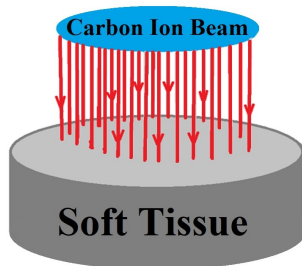


**Figure 1:** Schematic of the simulated geometry.

### 2.2 GEANT4 toolkit simulation of carbon ions interaction with soft tissues

In the present study version 11.1.1 of the GEANT4 toolkit (with patch 01) was used to calculate the probability of producing secondary particles due to the interaction of carbon ions with soft tissue. The desired geometry in the simulation is a soft tissue phantom that carbon ions are irradiated on with the energies that listed in Table 1. In the INCLUDE and SRC folder, the detector construction library has been used to create the desired geometry that according to Fig. 1 is a cylinder soft tissue phantom with a 2 cm radius and variable thickness. To define the circle surface carbon ion source with a 1 cm radius and its energies, the primary detector construction library was used with G4ParticleTable-GetParticleTable()->FindParticle() command. To calculate the produced particles, the BeginOfRunAction function in the RunAction class was used, and to display the produced particles, the UserSteppingAction function was incorporated in the SteppingAction class. The FTFP_BERT physics package was used for spallation processes. The number of primary particles for simulation was $10^8$ particles to keep the relative error below 1%. By calculating the secondary particles produced from the primary particles, the probability of producing secondary particles due to one carbon ion in the soft tissue can be obtained. GEANT4 toolkit simulation is performed with a 3.0 GHz Core i5 laptop with 4 GB of RAM.

### 2.3 Beam divergence, beam Tail, and Range of carbon ion in soft tissue

The carbon ion beam divergence is a problem in cancer therapy that is due to the Coulomb interaction of carbon ions with soft tissue material. Carbon ion beam divergence is important for tumors in sensitive organs that damage the tissue surrounding the tumor. Previously the proton beam divergence was studied by Noshad et al. (Noshad and Givechi, 2005). In this work the carbon ion beam divergence in 1140 to 5180 MeV was studied by Monte Carlo simulation using MCNPX code and GEANT4 toolkit.

### 2.4 Dosimetry of secondary particle production by carbon ion in soft tissue

The dosimetry of secondary particles is important in ion therapy. The reason is that in addition to the dose caused by the ion beam, a second dose is also given to the patient in the tumor and surrounding tissues, which is effective in increasing the Relative Biological Effectiveness (RBE) in ion therapy (Nandy, 2021). The dose due to secondary particles needs to be determined accurately to assess this biological effect. For this matter, the energy of secondary particles is calculated by the GEANT4 toolkit, and the total energy of secondary particles produced in the soft tissue, the total energy of the secondary particles removed from the soft tissue, and their difference are calculated for secondary particle dose calculation.

## 3 Results and Discussion

The spallation yield results of secondary produced particles by carbon ion in soft tissue before internal tumors are investigated by MCNPX code and GEANT4 toolkit that are shown in the following. To calculate the secondary produced particle by carbon ion in soft tissue, first, the validation of the MCNPX code and GEANT4 toolkit must be checked and confirmed. For this purpose, the range of carbon ions in the soft tissue has been compared with the results calculated in this research.

### 3.1 The validity of the simulation

The range of carbon ions in soft tissues before the tumor shows the depth of it that expose to carbon ion radiation. By using the mesh tally in the MCNPX code and GEANT4 toolkit, the range of carbon ions can be obtained. Suit et al. (Suit et al., 2010) measured the carbon ion range in water as summarized in Table 1. The GEANT4 toolkit and MCNPX simulation result of carbon ion range in water for these energies were listed in Table 1.

A comparison of the carbon ion range with experimental and simulation results showed that the confidence level is 97% and 99% MCNPX and GEANT4 toolkit respectively.

**Table 2:** Carbon ion range, maximum energy in Bragg peak, beam divergence and tail in soft tissue. The data of this table have been taken from (Dudouet et al., 2014; Chen et al., 2014; Takahashi et al., 1998; Kim et al., 2015; Jain et al., 2020).

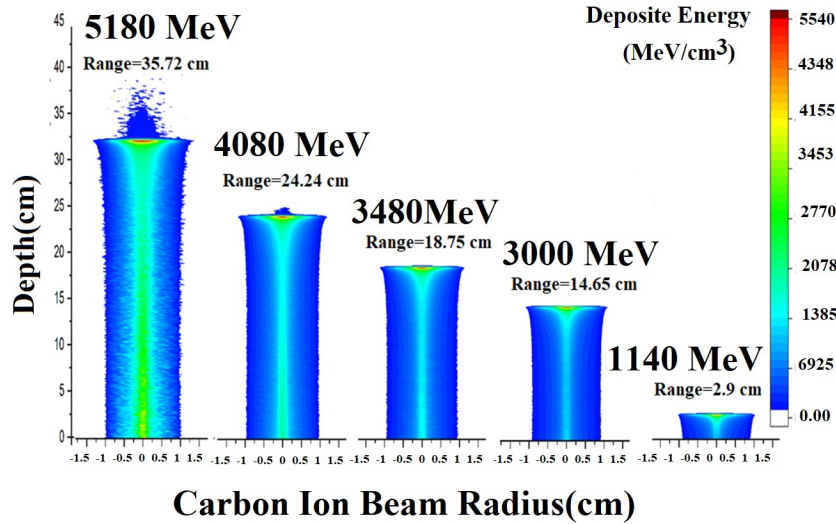| Carbon Energy (MeV.u$^{-1}$) | 95 | 250 | 290 | 340 | 430 |
|---|---|---|---|---|---|
| Carbon Energy (MeV) | 1140 | 3000 | 3480 | 4080 | 5160 |
| Range (cm) | $2.90 \pm 0.03$ | $14.65 \pm 0.15$ | $18.78 \pm 0.19$ | $24.24 \pm 0.24$ | $35.72 \pm 0.36$ |
| Maximum Energy (MeV.cm$^{-3}$) | $553.55 \pm 5.53$ | $328.94 \pm 3.29$ | $254.26 \pm 2.54$ | $192.96 \pm 1.93$ | $107.95 \pm 1.08$ |
| Bragg Peak (cm) | $2.65 \pm 0.03$ | $14.45 \pm 0.15$ | $18.55 \pm 0.19$ | $24.05 \pm 0.24$ | $35.35 \pm 0.35$ |
| Divergence (mm) | $4 \pm 0.04$ | $11 \pm 0.11$ | $14 \pm 0.14$ | $20 \pm 0.2$ | $33 \pm 0.3$ |
| Tail (cm) | 0 | 0 | $0.12 \pm 0.00$ | $1.01 \pm 0.01$ | $11 \pm 0.11$ |



**Figure 2:** Carbon ion beam divergence with tail in different ion energy with MCNPX code.

### 3.2 Result of beam divergence, tail, and range of carbon ion in soft tissue

After confirming the agreement of MCNPX code with measured values, the carbon ion range, maximum energy in Bragg peak region, and the beam divergence with tail in soft tissue by 1140, 3000, 3480, and 5160 MeV carbon ion energies were calculated by MCNPX code, and the results were shown in Fig. 2 and Table 2.
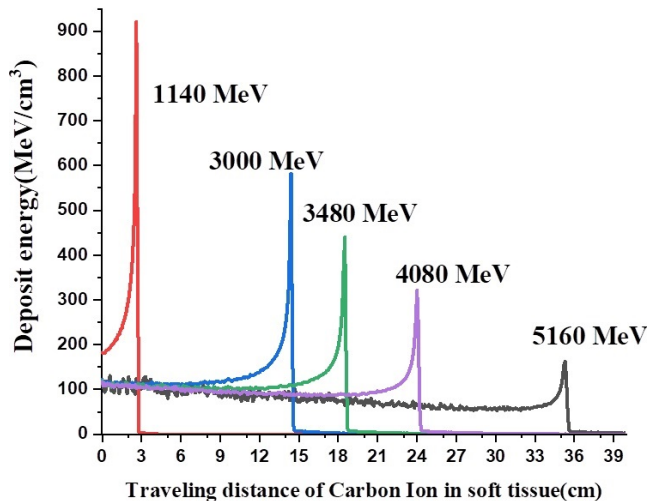


**Figure 3:** Carbon ion ranges in different energies with MC-NPX code.

The result of Table 2 shows that the range of carbon ions for 1140 to 5160 MeV are 2.90 to 35.72 cm in soft tissue that was shown up to 35.72 cm of soft tissue was affected before the tumor in carbon ion therapy. The energy transfers to unit volume (1 cm$^3$) of tumor depend on carbon ion energy and with an increase of energy from 1140 to 5160 MeV decrease from 553.55 to 107.95 MeV. The important parameter for carbon ion beam is beam divergence which increases with increasing energy for 1140 to 5160 MeV from 4 to 33 mm, respectively. The average distance of the Bragg peak point to the end of the range for 1140 to 5160 MeV carbon ion energy is 0.29 cm.

For high-energy carbon ions, the secondary particle productions cause the tail to be extended far away from the end of the range. The tail for 3480, 4080, and 5160 MeV of carbon ion energy are 0.12, 1.01, and 11 cm, respectively, and are more observable than others. The tail result for 3480 MeV ion carbon beam in depth vs dose distribution across T-175 flask that fill with Fricke gel as dosimeter was shown a 0.2 cm tail at 14.5 cm range (Buglewicz et al., 2019) that is in the range of tail in soft tissue by 3480 MeV ion beam (0.12 cm). The carbon-ion fragmentation tail, can continue travelling at nearly the same velocity and direction beyond the carbon-ion Bragg peak. Therefore, because of the carbon-ion sharp narrow Bragg peak and dose from the nuclear fragmentation, the extent of cell damage surrounding the Bragg peak remains unclear and must be addressed to further understand the precision of carbon-ion biological dose distribution and

**Table 3:** MCNPX result of the SPPY(#/(cm3.sp)) in soft tissue by 5160 MeV carbon ions.

| N | Z | SPPY | N | Z | SPPY | N | Z | SPPY | N | Z | SPPY | N | Z | SPPY |
|---|---|------|---|---|------|---|---|------|---|---|------|---|---|------|
| 4 | 2 | 0.01355 | 6 | 5 | 0.1292 | 9 | 6 | 3E-4 | 10 | 9 | 5E-5 | 14 | 15 | 2E-4 |
| 6 | 2 | 9E-4 | 5 | 7 | 8E-4 | 5 | 7 | 1.5E-4 | 10 | 10 | 1E-4 | 16 | 14 | 5E-5 |
| 3 | 3 | 0.11215 | 8 | 5 | 0.0012 | 6 | 7 | 0.01185 | 10 | 11 | 1.5E-4 | 15 | 15 | 1E-4 |
| 4 | 3 | 0.0741 | 3 | 6 | 0.00205 | 7 | 7 | 0.02905 | 12 | 10 | 2.5E-4 | 15 | 15 | 5E-4 |
| 5 | 3 | 0.00985 | 4 | 6 | 0.0051 | 8 | 7 | 0.07945 | 12 | 11 | 1.5E-4 | 16 | 16 | 5E-5 |
| 6 | 3 | 0.0018 | 5 | 3 | 0.0151 | 7 | 9 | 5E-5 | 13 | 11 | 5E-5 | 17 | 16 | 5E-5 |
| 3 | 4 | 0.0968 | 5 | 4 | 2E-4 | 10 | 7 | 5E-5 | 12 | 12 | 5E-5 | 18 | 16 | 2.5E-4 |
| 4 | 4 | 0.00105 | 5 | 6 | 0.1197 | 5 | 8 | 0.00145 | 14 | 12 | 5E-5 | 17 | 17 | 1E-4 |
| 5 | 4 | 0.0244 | 6 | 6 | 0.0336 | 6 | 8 | 0.01425 | 14 | 13 | 5E-5 | 19 | 18 | 1.5E-4 |
| 6 | 4 | 0.01255 | 7 | 6 | 0.01845 | 7 | 8 | 0.07475 | 13 | 14 | 1E-4 | 20 | 18 | 2E-4 |
| 9 | 4 | 1E-4 | 8 | 6 | 0.01365 | 9 | 8 | 1E-4 | 14 | 14 | 1.5E-4 | 19 | 19 | 2E-4 |
| 5 | 5 | 0.04815 | 8 | 8 | 5E-4 | - | - | - | - | - | - | - | - | - |

help define the extent of unwanted cellular damage surrounding its Bragg peak (Buglewicz et al., 2019).

Also, this research aimed to calculate the secondary particles or damage yield in soft tissue by calculation of spallation production with carbon ions. The damage or spallation yield in soft tissue by calculation of spallation production with carbon ions was carried out by MCNPX code and GEANT4 toolkit.

# 4 The MCNPX result of secondary particle production yield (SPPY) in soft tissue

The neutron and proton numbers (N and Z) of secondary particle production in soft tissue before tumors by 5160 MeV carbon ions energy is investigated by MCNPX simulation and the result of SPPY are shown in Table 3. The SPPY was defined as the number of secondary particle production (#) in unit volume (1 cm$^3$) of a target for one proton irradiation (sp) (#/(cm3.sp)).

The results of Table 3 show the atomic number (Z) and mass number (A) of secondary particles produced by carbon ions with 430 MeV.u$^{-1}$ (5160 MeV) energy. The Z number is between 2 to 19. The SPPY for Z between 4 to 5 is larger than others. According to Table 3 data, the radioactive particles produced in soft tissue before the tumor in carbon ion therapy by MCNPX code spallation and activation processes were shown in Table 4.

**Table 4:** The radioactive elements produced in soft tissue by carbon ion using MCNPX code.

| Element | Decay mode | Half-life |
|---------|-----------|-----------|
| Be-7 | $\varepsilon$ | 53.12 d |
| Be-10 | $\beta^-$ | 1.51E+6 y |
| C-11 | $\varepsilon^+\beta^+$ | 20.39 m |
| C-14 | $\beta^-$ | 5730 y |
| N-13 | $\varepsilon^+\beta^+$ | 9.965 m |
| F-18 | $\varepsilon^+\beta^+$ | 109.77 m |
| Ne-24 | $\beta^-$ | 3.38 m |
| P-30 | $\varepsilon^+\beta^+$ | 2.498 m |
| Cl-34 | $\varepsilon^+\beta^+$ | 32.00 m |
| Ar-37 | $\varepsilon$ | 35.04 d |
| K-38 | $\varepsilon^+\beta^+$ | 7.636 m |

Table 4 shows the MCNPX simulation result of long half-life radioactive elements production in soft tissue by carbon ion. The Ar-37, Be-10, Be-7, and C-14 radioactive elements with a long half-life that remains in the human body after treatment. if this radioisotopes enter the blood system then these deposited in bone marrow and cause genetic mutations and stem cell damage. Most radioactive elements are positron-emitters that annihilate gamma-rays which can be used for imaging during carbon ion therapy.

## 4.1 Comparison of SPPY in soft tissue and water by Carbon ion beam

Previously, secondary particles produced by 3240 MeV energy of carbon ion in water were simulated by the GEANT4 toolkit that atomic and mass numbers was between 0 to 12 and 0 to 25, respectively (Hamad, 2021). The same atomic and mass numbers intervals of secondary particles produced by the 5160 MeV energy of carbon ions in soft tissue that calculated by MCNPX simulation was seen. The result of the MCNPX code was shown that the C-11 has the maximum SPPY by 5160 MeV energy of carbon ion beam in soft tissue. But O-17 has the maximum Yield by 3240 MeV energy of carbon ion beam in water (Hamad, 2021).

## 4.2 The GEANT4 toolkit result of SPPY in soft tissue by Carbon ions

The GEANT4 toolkit result of the SPPY in soft tissue by 1140, 3000, 3480, 4080, and 5160 MeV energy of carbon ion is investigated and the results are given in Table 5.

According to the results of Table 5, it can be seen that the isotopes of hydrogen, carbon, helium, nitrogen, boron, beryllium, calcium, argon, potassium, sulfur, sodium, silicon, and fluorine are the most abundant in the production of secondary particles by carbon ion. The results show that the SPPY of these isotopes increases with increasing carbon ion energy. The highest SPPY is related to hydrogen that increases from 1.31 to 9.13 with increasing the energy from 1140 MeV to 5160 MeV. The lowest yield ($1.11 \times 10^{-4}$) is related to Li-9, which is produced only for carbon ions with 5160 MeV energy. Except hydrogen,

**Table 5:** The GEANT4 toolkit result of SPPY in soft tissue by Carbon ions.

| Carbon Energy (MeV) | 5160 | | 4080 | | 3480 | | 3000 | | 1140 | |
|---|---|---|---|---|---|---|---|---|---|---|
| Particle | SPPY | Energy (MeV) | SPPY | Energy (MeV) | SPPY | Energy (MeV) | SPPY | Energy (MeV) | SPPY | Energy (MeV) |
| H-1 | 9.133925 | 7.7118 | 8.419888 | 5.0612 | 7.512878 | 3.8625 | 6.487996 | 3.0243 | 0.1312588 | 1.0115 |
| Neutron | 0.535301 | 113.53 | 0.423873 | 85.132 | 0.339897 | 71.202 | 0.263563 | 60.994 | 0.0033422 | 27.233 |
| C-12 | 0.524329 | 3.3659 | 0.486397 | 2.6825 | 0.435089 | 2.5365 | 0.375064 | 2.6673 | 0.007531 | 4.1853 |
| Gamma | 0.412967 | 3.4942 | 0.356823 | 2.659 | 0.306677 | 2.5693 | 0.256153 | 2.5468 | 0.0051366 | 2.4984 |
| He-4 | 0.250606 | 417.43 | 0.209485 | 308.46 | 0.17566 | 260.93 | 0.142184 | 230.21 | 0.0027801 | 117.87 |
| H-2 | 0.148443 | 161.58 | 0.131199 | 114.7 | 0.115196 | 90.782 | 0.096238 | 73.565 | 0.0020837 | 28.727 |
| N-14 | 0.104278 | 1.6136 | 0.095326 | 1.8127 | 0.084262 | 1.9919 | 0.071839 | 2.0923 | 0.0013758 | 4.5825 |
| e$^+$ | 0.04593 | 3.1476 | 0.038448 | 1.3366 | 0.032124 | 1.1739 | 0.026827 | 1.1308 | 0.000536 | 1.1201 |
| $\nu_e$ | 0.041822 | 1.7881 | 0.036342 | 1.1287 | 0.030456 | 1.1033 | 0.025369 | 1.0862 | 0.0005084 | 1.052 |
| N-15 | 0.041303 | 3.5623 | 0.034716 | 4.3777 | 0.028659 | 5.0969 | 0.023038 | 5.62 | 0.0003361 | 13.986 |
| B-11 | 0.029205 | 775.91 | 0.025773 | 543.63 | 0.021855 | 453.18 | 0.018637 | 383.73 | 0.0003835 | 171.9 |
| He-3 | 0.023508 | 529.67 | 0.019489 | 398.91 | 0.016335 | 329.45 | 0.01313 | 283.46 | 0.0003364 | 100.82 |
| H-3 | 0.021502 | 510.93 | 0.017581 | 380.93 | 0.014376 | 313.68 | 0.011323 | 270.51 | 0.0003072 | 93.667 |
| C-13 | 0.016777 | 6.4558 | 0.014976 | 7.4682 | 0.012567 | 8.2662 | 0.010401 | 8.2291 | 0.0001911 | 16.929 |
| O-15 | 0.016022 | 8.0267 | 0.012972 | 10.005 | 0.010171 | 11.817 | 0.00797 | 13.818 | 0.000097 | 39.126 |
| Li-6 | 0.01569 | 519.76 | 0.013149 | 387.61 | 0.01141 | 332.59 | 0.009054 | 304.05 | 0.0001798 | 166.12 |
| C-11 | 0.015293 | 1644 | 0.013261 | 1243 | 0.010882 | 1100 | 0.009492 | 974.72 | 0.0002072 | 545.31 |
| B-10 | 0.014876 | 810.73 | 0.013345 | 563.48 | 0.011356 | 461.72 | 0.009309 | 390.95 | 0.0001701 | 179.31 |
| $\bar{\nu}_e$ | 0.011566 | 1.6432 | 0.010344 | 1.5455 | 0.009269 | 1.6238 | 0.007802 | 1.6397 | 0.0001507 | 1.6541 |
| Li-7 | 0.009409 | 553.85 | 0.008894 | 359.78 | 0.007752 | 296.54 | 0.006251 | 257.22 | 0.0001287 | 125.13 |
| B-10 | 0.009024 | 1110 | 0.007632 | 830.45 | 0.006497 | 692.41 | 0.005246 | 623.71 | 0.000092 | 349.95 |
| Be-7 | 0.005726 | 886.71 | 0.004727 | 677.54 | 0.004069 | 583.74 | 0.003233 | 540.13 | 0.0000654 | 291.24 |
| N-13 | 0.003961 | 18.108 | 0.0033 | 20.847 | 0.002742 | 24.176 | 0.002282 | 27.531 | 0.0000458 | 57.418 |
| Cl-36 | 0.003626 | 0.04 | 0.003319 | 0.06 | 0.003054 | 0.01 | 0.002531 | 0.97 | 0.0000569 | 0.02 |
| Cl-35 | 0.003585 | 0.13 | 0.003262 | 0.05 | 0.002999 | 0.18 | 0.002648 | 0.19 | 0.0000486 | 0.38 |
| Ar-36 | 0.003581 | 0.03 | 0.003285 | 0.02 | 0.003002 | 0.07 | 0.002503 | 0.7 | 0.0000557 | 0 |
| Be-9 | 0.003548 | 740.15 | 0.003085 | 514.4 | 0.002546 | 409.72 | 0.00209 | 364.81 | 0.0000335 | 150.19 |
| C-14 | 0.002778 | 16.117 | 0.002334 | 18.842 | 0.001906 | 22.348 | 0.001637 | 24.478 | 0.0000267 | 47.45 |
| C-10 | 0.002602 | 1396 | 0.002115 | 1013 | 0.001752 | 825.36 | 0.001397 | 659.04 | 0.0000206 | 339.34 |
| O-18 | 0.002541 | 0.27 | 0.002322 | 0.82 | 0.002016 | 0.68 | 0.001832 | 0.89 | 0.0000478 | 3.8771 |
| O-14 | 0.002038 | 24.183 | 0.001759 | 30.353 | 0.00146 | 36.522 | 0.001207 | 42.198 | 0.0000169 | 76.825 |
| Be-10 | 0.001996 | 1035 | 0.001621 | 663.46 | 0.001311 | 563.07 | 0.001068 | 437.28 | 0.0000159 | 186.42 |
| $\pi^0$ | 0.001809 | 85.421 | 0.000196 | 72.739 | 0 | 0 | 0 | 0 | 0 | 0 |
| $\pi^+$ | 0.001756 | 96.403 | 0.000174 | 92.688 | 0 | 0 | 0 | 0 | 0 | 0 |
| P-31 | 0.001478 | 0.85 | 0.001153 | 0.23 | 0.001262 | 0.54 | 0.001097 | 0.5 | 0.0000225 | 1.9861 |
| $\pi^+$ | 0.001556 | 84.635 | 0 | 0 | 0 | 0 | 0 | 0 | 0 | 0 |
| O-17 | 0.001537 | 5.7427 | 0.001591 | 9.3981 | 0.001586 | 10.502 | 0.0016 | 15.131 | 0.0000709 | 36.997 |
| S-32 | 0.001264 | 0.36 | 0.001153 | 0.23 | 0.001028 | 0.4 | 0.00082 | 0.49 | 0 | 1.3519 |
| He-6 | 0.001203 | 288.46 | 0.00098 | 185.39 | 0.000868 | 170.92 | 0.000643 | 117.02 | 0 | 0 |
| Na-23 | 0.001059 | 0.58 | 0.000996 | 1.3278 | 0.000932 | 1.5421 | 0.000804 | 2.0713 | 0.0000191 | 7.8445 |
| $\nu_\mu$ | 0.001029 | 30.459 | 0.0001 | 29.994 | 0 | 0 | 0 | 0 | 0 | 0 |
| $\bar{\nu}_\mu$ | 0.001024 | 36.757 | 0.000101 | 35.319 | 0 | 0 | 0 | 0 | 0 | 0 |
| $\mu$ | 0.001007 | 5.8686 | 0 | 0 | 0 | 0 | 0 | 0 | 0 | 0 |
| Be-8 | 0.000975 | 0.01 | 0.000798 | 0.01 | 0.00071 | 0.01 | 0.000626 | 0.01 | 0 | 0 |
| Be-6 | 0.000861 | 541.07 | 0.000749 | 414.3 | 0.000614 | 375.22 | 0.000506 | 387.47 | 0 | 0 |
| Li-8 | 0.000816 | 537.07 | 0.000649 | 400.36 | 0.000513 | 292.03 | 0.000446 | 274.92 | 0 | 0 |
| N-12 | 0.000769 | 332.85 | 0.00067 | 310.88 | 0.000677 | 361.66 | 0.000577 | 272.11 | 0.0000149 | 226.9 |
| K-39 | 0.000724 | 0.12 | 0.000716 | 0.11 | 0.000581 | 0.36 | 0.000525 | 0.18 | 0.000012 | 0.57 |
| B-12 | 0.00064 | 70.409 | 0.000563 | 40.28 | 0.000568 | 38.235 | 0.000473 | 42.479 | 0 | 0 |
| N-16 | 0.00060 | 5.7172 | 0.000603 | 6.9944 | 0.000564 | 7.5829 | 0.00051 | 8.3889 | 0.0000135 | 16.224 |
| B-8 | 0.00042 | 755.57 | 0.000308 | 616.39 | 0.000273 | 411.71 | 0.000273 | 399.93 | 0 | 0 |
| N-16 | 0.00034 | 11.694 | 0.00034 | 16.783 | 0.000321 | 18.014 | 0.000269 | 18.015 | 0 | 0 |
| K-40 | 0.000237 | 0 | 0.000216 | 0.55 | 0.000207 | 93.189 | 0.000147 | 0.01 | 0 | 0 |
| Cl-37 | 0.000234 | 0.58 | 0.000211 | 0.13 | 0.000226 | 0.32 | 0.000191 | 0.33 | 0 | 0 |
| Ca-40 | 0.000208 | 0 | 0.000193 | 0.03 | 0.000191 | 0.28 | 0.000147 | 0.01 | 0 | 0 |
| Cl-36 | 0.0002 | 0.01 | 0.000182 | 0.01 | 0.000149 | 0.23 | 0.00013 | 0.01 | 0 | 0 |
| Be-8 | 0.000197 | 2.2174 | 0.000112 | 0.12 | 0 | 0 | 0 | 0 | 0 | 0 |
| Si-30 | 0.000194 | 1.2275 | 0.000166 | 2.5776 | 0.000152 | 1.7123 | 0.000129 | 2.4925 | 0 | 0 |
| S-33 | 0.000173 | 1.1799 | 0.000175 | 2.2205 | 0.000148 | 1.7959 | 0 | 0 | 0 | 0 |
| S-34 | 0.000155 | 1.3329 | 0.000114 | 1.4737 | 0.000101 | 1.3546 | 0 | 0 | 0 | 0 |
| F-17 | 0.000148 | 42.568 | 0.000221 | 47.34 | 0.00032 | 44.683 | 0.000327 | 47.317 | 0.0000238 | 91.377 |
| C-9 | 0.000146 | 1170 | 0.000115 | 682 | 0 | 0 | 0 | 0 | 0 | 0 |
| B-13 | 0.000142 | 45.295 | 0.000105 | 51.853 | 0.0001 | 59.389 | 0 | 0 | 0 | 0 |
| P-30 | 0.000139 | 5.4671 | 0.000108 | 4.4618 | 0.000105 | 5.4712 | 0 | 0 | 0 | 0 |
| Si-28 | 0.000125 | 7.6014 | 0 | 0 | 0 | 0 | 0 | 0 | 0 | 0 |
| Si-29 | 0.000125 | 5.5477 | 0 | 0 | 0.000107 | 8.1199 | 0 | 0 | 0 | 0 |
| C-15 | 0.000118 | 8.6942 | 0.000129 | 12.918 | 0.00014 | 22.735 | 0 | 0 | 0 | 0 |
| B-9 | 0.000116 | 0.03 | 0.000105 | 0.07 | 0 | 0 | 0 | 0 | 0 | 0 |
| Li-9 | 0.000111 | 984.93 | 0 | 0 | 0 | 0 | 0 | 0 | 0 | 0 |

**Table 6:** Mean energy and production yield of neutron and positron versus carbon ion energy in soft tissue.

| Carbon Ion Energy (MeV) | Neutron Production | | Positron Production | |
|---|---|---|---|---|
| | Medium Energy (MeV) | Neutron Yield ($\#.cm^{-3}.sp^{-1}$) | Medium Energy (MeV) | Neutron Yield ($\#.cm^{-3}.sp^{-1}$) |
| 1140 | $27.23 \pm 0.27$ | $0.03 \pm 0.00$ | $1.120 \pm 0.01$ | $5.36E\text{-}3 \pm 0.00$ |
| 3000 | $60.99 \pm 0.61$ | $0.26 \pm 0.00$ | $1.131 \pm 0.01$ | $0.03 \pm 0.00$ |
| 3480 | $71.20 \pm 0.71$ | $0.34 \pm 0.00$ | $1.17 \pm 0.01$ | $0.03 \pm 0.00$ |
| 4080 | $85.13 \pm 0.85$ | $0.42 \pm 0.00$ | $1.34 \pm 0.01$ | $0.04 \pm 0.00$ |
| 5160 | $113.53 \pm 1.13$ | $0.54 \pm 0.01$ | $3.15 \pm 0.01$ | $0.05 \pm 0.01$ |

**Table 7:** The GEANT4 toolkit results of the radioactive elements produced in soft tissue by carbon ion spallation.

| Radioactive Element | Half life | Radioactive Element | Half life | Radioactive Element | Half life |
|---|---|---|---|---|---|
| H-3 | 17.774 y | Na-22 | 3.7575 y | P-33 | 36.57 d |
| Be-7 | 76.78 d | Na-24 | 21.636 h | Cl-38 | 53.726 min |
| Be-10 | 2180000 y | Na-25 | 1.4211 min | Cl-34 | 46.152 min |
| C-11 | 29.379 min | Al-26 | 1035100 y | Cl-36 | 434980 y |
| C-14 | 8229 y | Al-28 | 3.2388 min | S-35 | 126.05 d |
| N-13 | 14.376 min | Al-29 | 9.4641 min | S-37 | 7.2856 min |
| O-14 | 1.6977 min | Mg-27 | 13.645 min | Ar-37 | 50.51 d |
| O-15 | 2.9392 min | Mg-28 | d 1.2572 | Ar-39 | 388.35 y |
| F-17 | 1.5507 min | Si-31 | 3.7837 h | K-38 | 11.016 min |
| F-18 | 2.6394 d | P-30 | 3.6039 min | K-40 | 1.8E+09 y |
| Neutron | 14.67 min | P-32 | 20.584 d | K-42 | 17.832 h |

the neutrons, C-12, and alpha particles have the highest SPPY.

The produced secondary particles have high kinetic energies. The highest kinetic energy related to C-10 with 1396 MeV energy. Also, neutrons with high radiation risk, have 27.23 to 113.53 MeV kinetic energy for 1140 to 5160 MeV carbon ions respectively. Most of them, in addition to reaching to body parts, can penetrate outside the treatment room. Meanwhile, gamma rays with an energy of 3.49 MeV, positrons with an energy of 3.15 MeV, neutrinos, muons, and pions are also produced with high energies in carbon therapy. Due to the high energies of positrons and gamma rays, they have high radiation risks. Results show that in the carbon therapy, 7 isotopes of carbon, 3 isotopes of hydrogen, 3 isotopes of helium, 6 isotopes of neon, 5 isotopes of boron, 4 isotopes of oxygen, 4 isotopes of lithium, 6 isotopes of beryllium, 4 isotopes of calcium, 2 isotopes of potassium, 3 isotopes of sulfur, 3 isotopes of silicon and argon and 1 isotope of sodium, phosphorus, fluorine, and calcium was produced in soft tissue. Some of these secondary particles are radioactive, which will be discussed in this paper. It should be noted that in Table 5 only report the secondary elements with yields larger than $10^{-4}$. According of Table 5, the gamma energy production in different carbon ion energy was shown that with increase energy the gamma yield increases (0.3) (Zarifi et al., 2019). In the list of secondary particles produced, there are neutrons and positrons whose mean energy and production yields versus carbon ion energy were shown in Table 6.

In the list of secondary produced particles, there are neutrons and positrons that mean energy and production yields versus carbon ion energy were shown in Table 6.

These neutrons and positrons that produced during carbon ion therapy usually deliver doses in healthy tissue outside the target volume. Though, the dose of this neutrons and positrons particles is small ,but secondary radiogenic cancer is probable in healthy tissues. Therefore the probability of secondary radiogenic cancer in carbon ion therapy is less than in photon therapy.

### 4.3 The GEANT4 toolkit result of radioactive elements production in soft tissue by Carbon ions

According to the Table 6 data, the GEANT4 toolkit results of the radioactive elements produced by spallation processes in soft tissue due carbon ions therapy were shown in Table 7.

The number of radioactive elements produced in soft tissue by carbon ion by the GEANT4 toolkit is 32 elements that is larger than the MCNPX results (11 elements). Therefore, the GEANT4 toolkit is more reliable for the investigation of radioactive elements produced by ions than the MCNPX code. The SPPY of radioactive elements generated by carbon ions in soft tissue were calculated by the GEANT4 toolkit and the results are summarized in Table 8.

The results of Table 8 show that H-3, C-11, O-15, Be-7, Cl-36, N-13, F-17, C-14, Be-10, F-18, Na-22, K-40, and Na-24 radioactive elements are produced with the highest SPPY in soft tissue by carbon ion spallation. With the increase in carbon ion energy, the production yield of these elements increases. The production yield of H-3, C-11, O-15, Be-7, Cl-36, N-13, F-17, C-14, and Be-10 is more than others. Also, the SPPY of neutrons with a 10 min half-life is larger than all radioactive elements production listed in Table 8. Neutrons decay into protons via

**Table 8:** The GEANT4 toolkit results of the SPPY of radioactive elements in soft tissue by carbon ion spallation.

| Carbon Energy (MeV) | 5160 | | 4080 | | 3480 | | 3000 | | 1140 | |
|---|---|---|---|---|---|---|---|---|---|---|
| Reaction | SPPY | Energy (MeV) | SPPY | Energy (MeV) | SPPY | Energy (MeV) | SPPY | Energy (MeV) | SPPY | Energy (MeV) |
| $^{35}$Cl$(2p,\gamma)^{37}$Ar | 22.525 | 0.000005 | 5.7967 | 0.000028 | 3.3537 | 0.000028 | 5.0857 | 0.00034 | 4.7637 | 0.000033 |
| $^{16}$O$(p,^{10}$B$)^7$Be | 291.24 | 0.000654 | 540.13 | 0.003233 | 583.74 | 0.004069 | 677.54 | 0.04727 | 886.71 | 0.005726 |
| $^{31P}(p,\alpha)^{28}$Mg | 0 | 0 | 0 | 0 | 0 | 0 | 38.714 | 0.00002 | 31.043 | 0.000002 |
| $^{32}$S$(p,\beta$n$)^{32}$P | 6.8095 | 0.00001 | 5.3756 | 0.000055 | 4.478 | 0.000053 | 3.6045 | 0.00068 | 1.2674 | 0.000069 |
| $^{32}$S$(p,\beta)^{33}$P | 57.489 | 0.000001 | 16.022 | 0.000004 | 5.2597 | 0.000004 | 6.9292 | 0.00013 | 6.8456 | 0.000014 |
| $^{35}$Cl$(p,\beta$n$)^{35}$S | 24.561 | 0.000003 | 2.632 | 0.000009 | 10.877 | 0.000019 | 1.2741 | 0.00009 | 9.2631 | 0.000015 |
| $^{39}$K$(p,^{22}$Na$)^{18}$F | 70.473 | 0.000117 | 46.487 | 0.00011 | 45.858 | 0.000113 | 43.644 | 0.00094 | 52.941 | 0.000052 |
| $^{23}$Na$(p,\beta)^{24}$Na | 12.154 | 0.000013 | 3.9465 | 0.000052 | 3.75 | 0.000064 | 2.1279 | 0.00065 | 1.2584 | 0.000051 |
| $^{31}$P$(p,2p)^{31}$Si | 0 | 0 | 6.6528 | 0.000008 | 7.3656 | 0.00001 | 2.5459 | 0.00007 | 8.011 | 0.000016 |
| $^{31}$P$(p,3p$n$)^{28}$Al | 0 | 0 | 0.77 | 0.000015 | 8.2581 | 0.000013 | 2.3995 | 0.00013 | 1.4425 | 0.000025 |
| $^{31}$P$(p,3p)^{29}$Al | 0 | 0 | 24.525 | 0.000006 | 29.715 | 0.000005 | 23.051 | 0.00003 | 4.7803 | 0.000006 |
| $^{14}$N$(p,\alpha)^{11}$C | 545.31 | 0.002072 | 974.72 | 0.009492 | 1100 | 0.010882 | 1243.3 | 0.13261 | 1644.4 | 0.015293 |
| $^{35}$Cl$(p,d)^{34}$Cl | 123.74 | 0.000002 | 3.4462 | 0.000009 | 1.0317 | 0.000008 | 2.4957 | 0.00014 | 7.78 | 0.000011 |
| $^{16}$O$(p,\gamma)^{17}$F | 91.377 | 0.000238 | 47.317 | 0.000327 | 44.683 | 0.00032 | 47.34 | 0.00221 | 42.568 | 0.000148 |
| $^{39}$k$(p,d)^{38}$K | 81.794 | 0.000001 | 3.1579 | 0.000021 | 5.3044 | 0.000029 | 1.3738 | 0.00025 | 2.7694 | 0.000036 |
| $^{31}$P$(p,^5$He$)^{27}$Mg | 0 | 0 | 6.4192 | 0.000001 | 3.7211 | 0.000001 | 0 | 0 | 19.092 | 0.000001 |
| $^{16}$O$(p,\alpha)^{13}$N | 57.418 | 0.000458 | 27.531 | 0.002282 | 24.176 | 0.002742 | 20.847 | 0.033 | 18.108 | 0.003961 |
| $^{23}$Na$(2p,2\beta)^{25}$Na | 172.21 | 0.000001 | 172.21 | 0.000001 | 172.21 | 0.000001 | 43.492 | 0.00002 | 172.21 | 0.000002 |
| $^{14}$N$(p,n)^{14}$O | 27.233 | 0.033422 | 60.994 | 0.263563 | 71.202 | 0.339897 | 85.132 | 4.23873 | 113.53 | 0.535301 |
| $^{14}$N$(p,\gamma)^{15}$O | 39.126 | 0.00097 | 13.818 | 0.00797 | 11.817 | 0.010171 | 10.005 | 0.12972 | 8.0267 | 0.016022 |
| $^{32}$S$(p,^3$He$)^{30}$P | 23.73 | 0.000012 | 11.48 | 0.000087 | 5.4712 | 0.000105 | 4.4618 | 0.00108 | 5.4671 | 0.000139 |
| $^{39}$K$(p,^6$Li$)^{37}$S | 0.54 | 0.000001 | 0 | 0 | 0 | 0 | 0.56 | 0.00001 | 0.35 | 0.000001 |
| $^{23}$Na$(3p,\beta)^{26}$Al | 10.253 | 0.00002 | 18.513 | 0.000031 | 12.624 | 0.000037 | 8.2901 | 0.00039 | 8.3539 | 0.000051 |
| $^{39}$K$(p,^3$H$)^{39}$Ar | 68.449 | 0.000002 | 1.4742 | 0.000011 | 6.3631 | 0.000012 | 0 | 0 | 5.3726 | 0.000006 |
| $^{12}$C$(p, 3p)^{10}$Be | 186.42 | 0.000159 | 437.28 | 0.001068 | 563.07 | 0.001311 | 663.46 | 0.01621 | 1035.2 | 0.001996 |
| $^{16}$O$(p,3p)^{14}$C | 47.45 | 0.000267 | 24.478 | 0.001637 | 22.348 | 0.001906 | 18.842 | 0.02334 | 16.117 | 0.002778 |
| $^{35}$Cl$(p,$pn$\gamma)^{36}$Cl | 0.02 | 0.000569 | 0.11 | 0.002531 | 0.01 | 0.003054 | 0.06 | 0.03319 | 0.04 | 0.003626 |
| $^{39}$K$(p,$pn$\gamma)^{40}$K | 0 | 0.000027 | 0.003 | 0.000147 | 0 | 0.000207 | 0.55 | 0.00216 | 0 | 0.000237 |
| $^{23}$Na$(p,d)^{22}$Na | 23.006 | 0.000053 | 15.839 | 0.000066 | 15.349 | 0.000084 | 16.854 | 0.00065 | 6.8548 | 0.00008 |
| $^3$H: $^{39}$K$(p,3p)^{39}$Ar | 93.667 | 0.003072 | 270.51 | 0.011323 | 313.68 | 0.014376 | 380.93 | 0.17581 | 510.93 | 0.021502 |

beta-particle emission in the patient's body during carbon therapy. Some of these radioactive elements have a short half-life and it is necessary to keep the patient under treatment in the hospital before reaching the activity level limit. Some of these elements have a relatively long half-life in the patients and it is necessary to keep their distance from other people at home. Some of them have a long half-life also remain in the patient's body and have long-term radiation risks. In general, all produced radioactive elements after cancer treatment create short, medium, and long term radiation risks in the patient's body and are considered harmful.

## 5 Reactions description for radioisotopes production by proton spallation

The interaction of the proton with the nucleus of various elements in the soft tissue in the first stage creates a compound nucleus that its reaction can be shown as $^1_1P +^A_Z X \rightarrow {}^{A+1}_{Z+1}Y^*$. Usually, the compound nucleus is in an excited state. The compound nucleus can decay by either emission of various particles including protons, neutrons, alpha, deuterons, gamma, etc. or by the spallation process. In the spallation process, the compound nucleus is converted into a range of different particles with mass numbers smaller than the target. The Table 8 shows all spallation and emission particles by proton interaction with soft tissue elements that produced by (p,$\gamma$), (2p,$\gamma$), (p,He-3), (p,$\alpha$), (p,He-5), (p,3p), (p,d), (p,H-3), (p,2p), (3p,$\beta$), (2p,2$\beta$), (p,$\beta$), (p,n), (p,$\beta$n), (p,Li-6), (p,Na-22), (p,B-10), (p,3pn) and (n, $\gamma$) interactions. Gamma emission reactions (p,$\gamma$) occur in $^{14}$N(p,$\gamma)^{15}$O, $^{16}$O(p,$\gamma)^{17}$F and $^{35}$Cl(2p,$\gamma)^{37}$Ar reactions. Also, there are secondary neutron absorption reactions produced in compound nucleus decay and spallation, and there are also reactions that lead to gamma emission, which can be mentioned as $^{39}$K(n,$\gamma)^{40}$K, $^{35}$Cl(n,$\gamma)^{36}$Cl. The reactions that lead to the emission of alpha particles and its isotopes can be shown as $^{32}$S(p,He-3)$^{30}$P, $^{16}$O(p,$\alpha)^{13}$N, $^{31}$P(p,He-5)$^{27}$Mg, $^{14}$N(p,$\alpha)^{11}$C and $^{31}$P(p,a)$^{28}$Mg reactions. It is also possible to react the proton with the nucleus of the elements in the soft tissue where hydrogen and its isotopes are produced that are shown as $^{39}$K(p,3p)$^{39}$Ar, $^{23}$Na(p,d)$^{22}$Na, $^{16}$O(p,3p)$^{14}$C, $^{12}$C(p,3p)$^{10}$Be, $^{39}$K(p,H-3)$^{39}$Ar, $^{39}$k(p,d)$^{38}$K, $^{35}$Cl(p,d)$^{34}$Cl, $^{31}$P(p,3p) and $^{31}$P(p,2p)$^{31}$Si interaction in Table 8. Interactions that lead to beta production also include as $^{23}$Na(3p, )$^{26}$Al, $^{23}$Na(2p,2$\beta)^{25}$Na, $^{23}$Na (p,$\beta)^{24}$Na intractions. Proton interactions with soft tissue that cause neutron production also include $^{14}$N(p,n)$^{14}$O interaction. Interactions that cause the emission of multiple particles also include the $^{35}$Cl(p,$\beta$n)$^{35}$S, $^{32}$S(p,$\beta$n)$^{32}$P interactions in which both beta particles and neutrons are emitted. According to the results of the Table 8, it is possible to mention the of $^{39}$K(p,6Li)$^{37}$S, $^{39}$K(p,Na-22)$^{18}$F and $^{16}$O(p,B-10)$^7$Be reactions in which spallation interaction and activation by protons can be produced nuclei with mass numbers smaller than the initial nucleus. Probability of $^{39}$K(p,Li-6)$^{37}$S interaction at 4080 MeV proton energy is

**Table 9:** Secondary particles leakage from soft tissue in carbon ion therapy.

| Carbon Energy (MeV) | 1140 | | 3000 | | 3480 | | 4080 | | 5160 | |
|---|---|---|---|---|---|---|---|---|---|---|
| Particle | Energy (MeV) | Number | Energy (MeV) | Number | Energy (MeV) | Number | Energy (MeV) | Number | Energy (MeV) | Number |
| Gamma | 1.6959 | 0.038824 | 1.7782 | 0.201142 | 1.812 | 0.243285 | 1.8994 | 2.87091 | 2.6456 | 0.334364 |
| Neutron | 34.276 | 0.013557 | 74.019 | 0.15351 | 84.897 | 0.208768 | 99.877 | 2.74758 | 130.89 | 0.369342 |
| $\nu_e$ | 1.052 | 0.005084 | 1.0862 | 0.025369 | 1.1033 | 0.030456 | 1.1287 | 0.36342 | 1.7881 | 0.041822 |
| $\bar{\nu}_e$ | 1.6541 | 0.001507 | 1.6397 | 0.007802 | 1.6238 | 0.009269 | 1.5455 | 0.10344 | 1.6432 | 0.011566 |
| H-1 | 54.306 | 0.000147 | 109.73 | 0.020259 | 124.27 | 0.04292 | 143.4 | 0.83942 | 183.42 | 0.173965 |
| H-2 | 120.11 | 0.000022 | 240.48 | 0.00986 | 294.5 | 0.015764 | 371.21 | 0.22187 | 517.63 | 0.03037 |
| $e^+$ | 2.6079 | 0.000014 | 0 | 0 | 5.8639 | 0.000179 | 12.026 | 0.00282 | 26.622 | 0.000994 |
| H-3 | 148.23 | 0.000013 | 391.3 | 0.003012 | 473.23 | 0.004295 | 577.85 | 0.06313 | 773.71 | 0.008897 |
| alpha | 0 | 0 | 303.02 | 0.005783 | 423.96 | 0.016266 | 574.91 | 0.31403 | 841.76 | 0.058768 |
| C-12 | 0 | 0 | 0 | 0 | 0 | 0 | 71.221 | 0.00001 | 219.72 | 0.020376 |
| H-3 | 0 | 0 | 229.81 | 0.000561 | 296.05 | 0.002117 | 393.72 | 0.05022 | 608.91 | 0.009904 |
| $e^-$ | 2.0716 | 0.000421 | | 0.002327 | 2.334 | 0.002685 | 3.0098 | 0.03422 | 7.6848 | 0.004434 |
| B-10 | 0 | 0 | 0 | 0 | 0 | 0 | 0 | 0 | 905.96 | 0.00264 |
| Be-7 | 0 | 0 | 31.954 | 0 | 174.45 | 0.000001 | 288.51 | 0.00007 | 768.54 | 0.001264 |
| $\nu_\mu$ | 0 | 0 | 43.465 | 0.000003 | 30.964 | 0.00002 | 29.994 | 0.001 | 30.459 | 0.001264 |
| $\bar{\nu}_\mu$ | 0 | 0 | | 0.000004 | 35.733 | 0.00002 | 35.319 | 0.00101 | 36.757 | 0.001024 |
| $\pi^+$ | 0 | 0 | 0 | 0 | 76.3 | 0.000004 | 92.823 | 0.00045 | 90.427 | 0.000469 |
| B-10 | 0 | 0 | 0 | 0 | 0 | 0 | 0 | 0 | 885.03 | 0.000393 |
| $\pi^-$ | 0 | 0 | 90.073 | 0.000001 | 116.09 | 0.000009 | 75.462 | 0.00034 | 88.302 | 0.000318 |
| C-11 | 0 | 0 | 0 | 0 | 0 | 0 | 0 | 0 | 170.1 | 0.000091 |
| $\mu^+$ | 0 | 0 | 0 | 0 | 1.812 | 0 | 46.902 | 0.00001 | 63.136 | 0.000014 |
| $\mu^-$ | 0 | 0 | 27.961 | 0.000001 | 0 | 0 | 0 | 0 | 51.153 | 0.000009 |
| B-8 | 1.6959 | 0.038824 | 1.7782 | 0.201142 | 0 | 0.243285 | 1.8994 | 2.87091 | 2.6456 | 0.334364 |
| N-14 | 34.276 | 0.013557 | 74.019 | 0.15351 | 84.897 | 0.208768 | 99.877 | 2.74758 | 130.89 | 0.369342 |
| C-10 | 1.052 | 0.005084 | 1.0862 | 0.025369 | 1.1033 | 0.030456 | 1.1287 | 0.36342 | 1.7881 | 0.041822 |
| N-12 | 1.6541 | 0.001507 | 1.6397 | 0.007802 | 1.6238 | 0.009269 | 1.5455 | 0.10344 | 1.6432 | 0.011566 |
| C-13 | 54.306 | 0.000147 | 109.73 | 0.020259 | 124.27 | 0.04292 | 143.4 | 0.83942 | 183.42 | 0.173965 |
| N-13 | 120.11 | 0.000022 | 240.48 | 0.00986 | 294.5 | 0.015764 | 371.21 | 0.22187 | 517.63 | 0.03037 |
| N-15 | 2.6079 | 0.000014 | 0 | 0 | 5.8639 | 0.000179 | 12.026 | 0.00282 | 26.622 | 0.000994 |
| O-16 | 148.23 | 0.000013 | 391.3 | 0.003012 | 473.23 | 0.004295 | 577.85 | 0.06313 | 773.71 | 0.008897 |
| B-11 | 0 | 0 | 303.02 | 0.005783 | 423.96 | 0.016266 | 574.91 | 0.31403 | 841.76 | 0.058768 |
| Li-6 | 0 | 0 | 0 | 0 | 0 | 0 | 71.221 | 0.00001 | 219.72 | 0.020376 |
| Li-7 | 0 | 0 | 229.81 | 0.000561 | 296.05 | 0.002117 | 393.72 | 0.05022 | 608.91 | 0.009904 |
| Be-9 | 2.0716 | 0.000421 | 2.25 | 0.002327 | 2.334 | 0.002685 | 3.0098 | 0.03422 | 7.6848 | 0.004434 |
| Be-10 | 0 | 0 | 0 | 0 | 0 | 0 | 0 | 0 | 905.96 | 0.00264 |
| He-6 | 0 | 0 | 0 | 0 | 174.45 | 0.000001 | 288.51 | 0.00007 | 768.54 | 0.001264 |
| Li-8 | 0 | 0 | 0 | 0.000003 | 30.964 | 0.00002 | 29.994 | 0.001 | 30.459 | 0.001029 |
| Li-9 | 0 | 0 | 31.954 | 0.000004 | 35.733 | 0.00002 | 35.319 | 0.00101 | 36.757 | 0.001024 |
| He-8 | 0 | 0 | 43.465 | 0 | 76.3 | 0.000004 | 92.823 | 0.00045 | 90.427 | 0.000469 |
| B-12 | 0 | 0 | 0 | 0 | 0 | 0 | 0 | 0 | 885.03 | 0.000393 |
| Be-11 | 0 | 0 | 90.073 | 0.000001 | 116.09 | 0.000009 | 75.462 | 0.00034 | 88.302 | 0.000318 |

also larger than other. Also, the probability of $^{16}$O(p,B-10)$^7$Be reaction increases with increasing energy. In 4080 MeV energy, the probability of $^{16}$O(p,B-10)$^7$Be reaction is higher than other. The energy of Be-7 produced particles is also significant and increases with increasing energy.The same behavior is observed for the interaction of $^{39}$K(p,Na-22)$^{18}$F. Finally, in the interaction of $^{31}$P(p,3pn)$^{28}$Al, the P-31 nucleus emits one neutron particle and three proton particles by absorbing a proton and turns into a Al-28 nucleus.

## 5.1 The GEANT4 toolkit result of secondary particles leakage from soft tissue in carbon ion therapy

Due to the high energy of the secondary particles, some of them move in soft tissue and reach far away from the production point (described as the tail). According to the results of Fig. 1, the tail is observable for carbon ions with high energy. In order to check the penetration depths of these particles, a slab of soft tissue with dimensions of

$1 \times 1 \times 1$ cm$^3$ is considered and the secondary particle escapes are calculated using the GEANT4 toolkit and results are given in Table 9.

According to the results of Table 9, the number of particles escaping the soft tissue depends on the carbon ion energy. For carbon ion with an energy of 1140 MeV, the gamma rays, electrons, neutrons, positrons, neutrinos, and hydrogen isotopes may escape the soft tissue, but at higher energies, the escaped particles were increased and there are a possibility for leakage of oxygen out of soft tissue. The passages of secondary particles out of the production region indicate the damage of healthy tissues by carbon ions.

## 5.2 Dosimetry of secondary produced particles per carbon ion in soft tissue by GEANT4 toolkit

By using the energy spectrum of secondary particles produced in carbon ion therapy up to 5160 MeV energy, it is possible to calculate the dose of secondary produced par-

**Table 10:** The secondary particle dose in soft tissues per carbon ion versus carbon ion energy.

| The secondary particle dose calculation steps | Carbon ion energy (MeV) | | | | |
|---|---|---|---|---|---|
| | 1140 | 3000 | 3480 | 4080 | 5160 |
| Leakage energy of secondary particles per carbon ion (MeV) | $0.55 \pm 0.06$ | $19.43 \pm 0.19$ | $37.92 \pm 0.38$ | $73.20 \pm 0.73$ | $177.69 \pm 0.178$ |
| Production energy of secondary particles per carbon ion | $10.95 \pm 1.10$ | $117.49 \pm 1.18$ | $166.99 \pm 1.67$ | $238.58 \pm 2.39$ | $387.30 \pm 3.387$ |
| The Absorbed energy of secondary particles per carbon ion (MeV) | $10.40 \pm 1.00$ | $98.06 \pm 0.98$ | $129.08 \pm 1.29$ | $165.37 \pm 1.65$ | $209.60 \pm 2.10$ |
| Energy percentage of secondary particles leakage per carbon ion | $0.05 \pm 0.00$ % | $0.65 \pm 0.01$ % | $1.09 \pm 0.01$ % | $1.79 \pm 0.02$ % | $3.44 \pm 0.03$ % |
| Energy percentage of secondary particles production per carbon ion | $0.96 \pm 0.01$ % | $3.92 \pm 0.04$ % | $4.79 \pm 0.05$ % | $5.85 \pm 0.06$ % | $7.51 \pm 0.07$ % |
| Energy percentage of secondary particles absorbed per carbon ion | $0.91 \pm 0.01$ % | $3.27 \pm 0.03$ % | $3.71 \pm 0.04$ % | $4.05 \pm 0.04$ % | $4.06 \pm 0.04$ % |
| Secondary particles dose per carbon ion (nGy) | $1.66 \pm 0.02$ | $15.74 \pm 0.16$ | $20.73 \pm 0.21$ | $26.52 \pm 0.27$ | $33.54 \pm 0.34$ |

ticles per carbon ion. According to the energy data of the secondary particles and the mass of the unit volume of soft tissue, the dose of secondary particles in soft tissues can be obtained and result was listed in Table 10.

The results of Table 10 show that by increasing the energy of carbon ions from 1140 MeV to 5160 MeV, the secondary dose delivered by secondary produced particles in soft tissue increases from 1.66 to 3.54 nGy. As a result, the dose of the secondary particles depends on the carbon ion energy and beam intensity.

# 6    Conclusions

In this study,the secondary particles and radioisotopes produced in soft tissue during carbon ion therapy were studied. Monte Carlo result was shown that theH-3, C-11, O-15, Be-7, Cl-36, N-13, F-17, C-14, Be-10, F-18, Na-22, K-40, and Na-24 radioactive elements exhibit the highest yield in soft tissue by carbon ion. Also, P-33, Cl-6, Ar-39, K-40, H-3, Be-10, and C-14 radioactive elements are important due to their longer half-lives than others. The K-42, Na-24, and Si-31 radioactive elements with half-lives of less than 24 h caused patients to be activated for many hours after carbon ion therapy. Thus it is inferred that after carbon ion therapy the patient must be quarantined in the hospital for at least one day. Therefore, in the treatment of cancerous tumors with carbon ions, because of radioactive element production,the healthy tissues are at high risk and have high radiation hazards. In the present work, a complete list of nuclear reactions that produce positron emitter nuclides are presented. The produced particles include positrons and neutrons, which are important in therapeutic dose verification with PET imaging, have an extra dose to the treatment environment. Due to the absorbed dose by the patients and radiotherapy personnel, it is important to estimate the neutron yield in charged particles therapy. The GEANT4 toolkit results of secondary-particle leakage from soft tissues in carbon ion therapy was shown that the gamma rays, electrons, neutrons, positrons, neutrinos, oxygen, and hydrogen isotopes escape from soft tissue to treatment room. The leakage of secondary particles out of soft tissue indicates damage to healthy tissues by the carbon ion beam. Also, the dose calculations of secondary particles produced per one car-

bon ion in soft tissue were performed with the GEANT4 toolkit. The secondary dose caused by secondary particles produced in soft tissue is up to 3.54 nGy per carbon ion. Dosimetry of secondary particles is important in ion therapy, because, in addition to the dose caused by the ion beam, a second dose is also delivered to the patient in the tumor and surrounding tissues, which increases the RBE during carbon ion therapy. In the case of high-energy carbon ions, there are tails after the Bragg curves that show penetration of secondary produced particels far away from the end of the carbon range. The tails for 3480, 4080, and 5160 MeV of carbon ion energy are 0.12, 1.01, and 11 cm, respectively.

The important parameter for carbon ion beam is beam divergence which increases with increasing energy. The beam divergence for 5160 MeV carbon ion is reported to be 33 mm.

# Conflict of Interest

The authors declare no potential conflict of interest regarding the publication of this work.

# References

Alanazi, N., Alanazi, R., Akhdar, H., et al. (2022). Monte carlo model for evaluation of concentration of gold nanoparticle clusters as predictor of effective dose in proton therapy of microscopic tumors. *AIP Advances*, 12(10):105014.

Allodji, R. S., Tucker, M. A., Hawkins, M. M., et al. (2021). Role of radiotherapy and chemotherapy in the risk of leukemia after childhood cancer: an international pooled analysis. *International Journal of Cancer*, 148(9):2079–2089.

Anikin, M., Lebedev, I., Naymushin, A., et al. (2020). Feasibility study of using IRT-T research reactor for BNCT applications. *Applied Radiation and Isotopes*, 166:109243.

Buglewicz, D. J., Banks, A. B., Hirakawa, H., et al. (2019). Monoenergetic 290 MeV/n carbon-ion beam biological lethal dose distribution surrounding the Bragg peak. *Scientific Reports*, 9(1):1–9.

Chen, Y.-J. and Paul, A. C. (2007). Compact proton accelerator for cancer therapy. In *2007 IEEE Particle Accelerator Conference (PAC)*, pages 1787–1789. IEEE.

Chen, Z., Hu, Z.-G., Chen, J.-D., et al. (2014). A simulation study of a dual-plate in-room PET system for dose verification in carbon ion therapy. *Chinese Physics C*, 38(8):088202.

Cheng, H.-G. and Feng, Z.-Q. (2021). Light fragment and neutron emission in high-energy proton induced spallation reactions. *Chinese Physics C*, 45(8):084107.

Chhura, L., Singh, D., Giri, P. K., et al. (2022). Production of dy-157 from n-14 induced reaction. In *Proceedings of the DAE Symp. on Nucl. Phys*, volume 66, page 545.

de Freitas Nascimento, L., Leblans, P., van der Heyden, B., et al. (2022). Characterisation and quenching correction for an Al2O3: C Optical Fibre Real Time System in Therapeutic Proton, Helium, and Carbon-Charged Beams. *Sensors*, 22(23):9178.

Didi, A., Dadouch, A., Bencheikh, M., et al. (2019). New study of various target neutron yields from spallation reactions using a high-energy proton beam. *International Journal of Nuclear Energy Science and Technology*, 13(2):120–137.

Dudouet, J., Cussol, D., Durand, D., et al. (2014). Benchmarking geant4 nuclear models for hadron therapy with 95 MeV/nucleon carbon ions. *Physical Review C*, 89(5):054616.

Gogineni, E., Bloom, B., Molina, F. D., et al. (2021). Radiotherapy dose escalation on pelvic lymph node control in patients with cervical cancer. *International Journal of Gynecologic Cancer*, 31(4).

Hamad, M. K. (2021). Bragg-curve simulation of carbon-ion beams for particle-therapy applications: A study with the GEANT4 toolkit. *Nuclear Engineering and Technology*, 53(8):2767–2773.

Hassanein, A., Hassan, M., Mohamed, N. M., et al. (2018). An optimized epithermal BNCT beam design for research reactors. *Progress in Nuclear Energy*, 106:455–464.

Ho, S. L., Choi, G., Yue, H., et al. (2020). In vivo neutron capture therapy of cancer using ultrasmall gadolinium oxide nanoparticles with cancer-targeting ability. *RSC Advances*, 10(2):865–874.

Iwata, Y., Shirai, T., Mizushima, K., et al. (2023). Design of a compact superconducting accelerator for advanced heavy-ion therapy. *Nuclear Instruments and Methods in Physics Research Section A: Accelerators, Spectrometers, Detectors and Associated Equipment*, 1053:168312.

Jablonska, P., Cambeiro, M., Gimeno, M., et al. (2021). Intraoperative electron beam radiotherapy and perioperative high-dose-rate brachytherapy in previously irradiated oligorecurrent gynecological cancer: Clinical outcome analysis. *Clinical and Translational Oncology*, 23:1934–1941.

Jain, A., Seth, P., Tripathi, A., et al. (2020). TL/OSL response of carbon ion beam irradiated NaMgF3: Tb. *Journal of Luminescence*, 222:117159.

Jäkel, O. (2020). Physical advantages of particles: protons and light ions. *The British journal of Radiology*, 93(1107):20190428.

Jowett, J. (2016). Lhc surpasses design luminosity with heavy ions. *CERN Courier*, 56(1):23–24.

Kasesaz, Y., Khalafi, H., and Rahmani, F. (2014). Design of an epithermal neutron beam for BNCT in thermal column of tehran research reactor. *Annals of Nuclear Energy*, 68:234–238.

Kayani, Z., Islami, N., Behzadpour, N., et al. (2021). Combating cancer by utilizing noble metallic nanostructures in combination with laser photothermal and X-ray radiotherapy. *Journal of Drug Delivery Science and Technology*, 65:102689.

Khezripour, S., Negarestani, A., and Rezaie, M. (2017). Investigating the response of Micromegas detector to low-energy neutrons using monte carlo simulation. *Journal of Instrumentation*, 12(08):P08007.

Kim, C. H., Lee, H.-R., Chang, S., et al. (2015). Practical biological spread-out Bragg peak design for a carbon beam. *Journal of the Korean Physical Society*, 67:1440–1443.

Kramer-Marek, G. and Capala, J. (2012). The role of nuclear medicine in modern therapy of cancer. *Tumor Biology*, 33:629–640.

Lin, Y., Huang, G., Huang, Y., et al. (2010). Process-Induced Cell Injury in Laser Direct Writing of Human Colon Cancer Cells. *Tissue engineering. Part C, Methods*.

Liu, W.-S., Changlai, S.-P., Pan, L.-K., et al. (2011). Thermal neutron fluence in a treatment room with a varian linear accelerator at a medical university hospital. *Radiation Physics and Chemistry*, 80(9):917–922.

Loap, P. and Kirova, Y. (2021). Fast Neutron Therapy for Breast Cancer Treatment: An Effective Technique Sinking into Oblivion. *International Journal of Particle Therapy*, 7(3):61–64.

Luo, Y., Huang, S.-C., Zhang, H., et al. (2023). Assessment of the induced radioactivity in the treatment room of the heavy-ion medical machine in wuwei using phits. *Nuclear Science and Techniques*, 34(2):29.

Masunaga, S.-i., Hirayama, R., Uzawa, A., et al. (2010). Influence of manipulating hypoxia in solid tumors on the radiation dose-rate effect in vivo, with reference to that in the quiescent cell population. *Japanese Journal of Radiology*, 28(2):132–142.

Nandy, M. (2021). Secondary Radiation in Ion Therapy and Theranostics: A Review. *Frontiers in Physics*, 8:598257.

Noshad, H. and Givechi, N. (2005). Proton therapy analysis using the Monte Carlo method. *Radiation Measurements*, 39(5):521–524.

Oancea, C., Granja, C., Marek, L., et al. (2023). Out-of-field measurements and simulations of a proton pencil beam in a wide range of dose rates using a Timepix3 detector: Dose rate, flux and LET. *Physica Medica*, 106:102529.

Ounoughi, N., Dribi, Y., Boukhellout, A., et al. (2022). Physical aspects of bragg curve of therapeutic oxygen-ion beam: Monte Carlo simulation. *Polish Journal of Medical Physics and Engineering*, 28(3):160–168.

Pasler, M., Georg, D., Wirtz, H., et al. (2011). Effect of photon-beam energy on VMAT and IMRT treatment plan quality and dosimetric accuracy for advanced prostate cancer. *Strahlentherapie und Onkologie*, 12(187):792–798.

Pshenichnov, I., Mishustin, I., and Greiner, W. (2005). Neutrons from fragmentation of light nuclei in tissue-like media: a study with the GEANT4 toolkit. *Physics in Medicine & Biology*, 50(23):5493.

Sauerwein, W., Moss, R., Stecher-Rasmussen, F., et al. (2011). Quality management in BNCT at a nuclear research reactor. *Applied Radiation and Isotopes*, 69(12):1786–1789.

Schippers, J., Duppich, J., Goitein, G., et al. (2006). The use of protons in cancer therapy at psi and related instrumentation. In *Journal of Physics: Conference Series*, volume 41, page 61. IOP Publishing.

Song, H., Kim, Y., and Sung, W. (2023). Modeling of the FLASH effect for ion beam radiation therapy. *Physica Medica*, 108:102553.

Stankovsky, A., Saito, M., Artisyuk, V., et al. (2001). Accumulation and transmutation of spallation products in the target of accelerator-driven system. *Journal of Nuclear Science and Technology*, 38(7):503–510.

Sudhakar, A. (2009). History of cancer, ancient and modern treatment methods. *Journal of Cancer Science & Therapy*, 1(2):1.

Suit, H., DeLaney, T., Goldberg, S., et al. (2010). Proton vs carbon ion beams in the definitive radiation treatment of cancer patients. *Radiotherapy and Oncology*, 95(1):3–22.

Takahashi, A., Yano, T., Matsumoto, H., et al. (1998). Effects of accelerated carbon-ions on growth inhibition of transplantable human esophageal cancer in nude mice. *Cancer Letters*, 122(1-2):181–186.

Wang, X., Xiao, J., and Jiang, G. (2021). Real time medical data monitoring and iodine-131 treatment of thyroid cancer nursing analysis based on embedded system. *Microprocessors and Microsystems*, 81:103660.

Washio, M., Hama, Y., Sakaue, K., et al. (2011). Fabrication of nano space controlled materials using high-energy heavy ion irradiation. Technical report.

Williams, T. J., MacDougall, G. J., Riemer, B. W., et al. (2023). SEEMS: A Single Event Effects and Muon Spectroscopy facility at the Spallation Neutron Source. *Review of Scientific Instruments*, 94(3).

Yoo, J. G. (1998). Neutron production from spallation reactions. In *Proceedings of the Korean Nuclear Society Conference*, pages 65–65. Korean Nuclear Society.

Zakalek, P., Doege, P.-E., Baggemann, J., et al. (2020). Energy and target material dependence of the neutron yield induced by proton and deuteron bombardment. In *EPJ Web of Conferences*, volume 231, page 03006. EDP Sciences.

Zarifi, M., Guatelli, S., Qi, Y., et al. (2019). Characterization of prompt gamma ray emission for in vivo range verification in particle therapy: A simulation study. *Physica Medica*, 62:20–32.